MAUSAM, **74**, 2 (April, 2023), 239-252

MAUSAM

DOI : https://doi.org/10.54302/mausam.v74i2.5948
Homepage: https://mausamjournal.imd.gov.in/index.php/MAUSAM

UDC No. 551.553.21 : 551.510.529

Global monsoon systems and their modulation by the equatorial Quasi-Biennial Oscillation

S. YODEN, V. KUMAR*, S. K. DHAKA* and M. H. HITCHMAN**

Institute for Liberal Arts and Sciences, Kyoto University, Kyoto, 606-8501, Japan

**Radio and Atmospheric Physics Lab, Rajdhani College, University of Delhi, New Delhi – 110 015, India*

***Department of Atmospheric & Oceanic Sciences, University of Wisconsin-Madison, WI, 53706, USA*

e mail : yoden.shigeo.53r@st.kyoto-u.ac.jp

सार – केवल तटस्थ ENSO अवधि (कुल 374 महीनों में) पर ध्यान केंद्रित करने के लिए ERA-अंतरिम पुनर्विश्लेषण, वर्षा, OLR, और SST के मासिक-औसत डेटा की 40 वर्षों (1979-2018) के लिए जांच की गई है ताकि विषुवतीय QBO द्वारा वैश्विक मॉनसून प्रणालियों के मॉडुलन को प्रकट किया जा सके। सबसे पहले, वैश्विक मॉनसून प्रणालियों के जलवायु विज्ञान को निचले क्षोभमंडलीय संचलन के देशांतर-अक्षांश भूखंडों और वार्षिक औसत तथा दो संक्रांति ऋतुओं के साथ-साथ दो मौसमों के बीच समग्र अंतर के साथ देखा जा सके। ITCZs की ऋतुनिष्ठव विविधताओं के अलावा, दो गोलार्धों के बीच वार्षिक चक्र के एक विपरीत चरण के साथ कई क्षेत्रीय मॉनसून प्रणालियों की अच्छी तरह से पहचान की जाती है। वर्षा से संबंधित मात्राएँ (OLR और विशिष्ट आर्द्रता), सतह की स्थितियाँ (MSLP और SST) और संचलन क्षेत्र से संबंधित नम संवहन प्रणालियां वैश्विक मॉनसून प्रणालियों की मूलभूत विशेषताओं को दर्शाती हैं। विषुवतीय निचले-समताप मंडल में आंचलिक-माध्य आंचलिक पवन विविधताओं के प्रमुख दो प्रमुख घटकों के आधार पर आठ QBO चरणों को शुरू करने के बाद, विपरीत QBO चरणों के लिए वर्षा और क्षोभमंडलीय संचलन में समग्र अंतर के सांख्यिकीय महत्व का मूल्यांकन किया जाता है। समग्र अंतर 20 और 50 hPa पर विषुवतीय क्षेत्रीय-औसत क्षेत्रीय पवन के पारंपरिक सूचकांकों के अनुरूप विशिष्ट QBO-चरणों के लिए सबसे बड़े परिमाण के साथ, क्षेत्रीय असममित घटकों के प्रभुत्व वाले कुछ क्षेत्रीय मॉनसून प्रणालियों में महत्वपूर्ण बदलाव दिखाते हैं। जोभूमध्य रेखा के साथ, महत्वपूर्ण QBO मॉडुलन पश्चिमी प्रशांत पर वाकर संचलन के मॉडुलन की विशेषता है। बोरियल ग्रीष्मा के दौरान मध्य अक्षांशों में, एक विशिष्ट QBO - चरण के लिए, उत्तरी-गोलार्ध केपश्चिमी प्रशांत महासागर में कम दबाव वाले चक्रवाती क्षोभ का सांख्यिकीय रूप से महत्वपूर्ण मॉडुलन प्राप्त होता है, जो चक्रवाती क्षोभ के पूर्वी हिस्से में भारी वर्षा की सांख्यिकीय रूप से महत्वपूर्ण विशेषताओं से जुड़ा होता है और इसके विपरीतपश्चिममें हल्की वर्षा होती है। बोरियल सर्दियों के दौरान, विशिष्ट चरणों के लिए उत्तरी-गोलार्ध पूर्वी प्रशांत और अटलांटिक में उत्तरी गोलार्ध के समान महत्वपूर्ण निम्न दबाव वाले चक्रवाती परिवर्तन पाए गए।

ABSTRACT. Monthly-mean data of ERA-Interim reanalysis, precipitation, outgoing longwave radiation (OLR) and sea surface temperature(SST) are investigated for 40 years (1979-2018) to reveal the modulation of the global monsoon systems by the equatorial quasi-biennial oscillation (QBO), focusing only on the neutral El Niño-Southern Oscillation (ENSO) periods (in total 374 months). First, the climatology of the global monsoon systems is viewed with longitude-latitude plots of the precipitation, its proxies and lower tropospheric circulations for the annual mean and two solstice seasons, together with the composite differences between the two seasons. In addition to seasonal variations of Intertropical Convergence Zones (ITCZs), several regional monsoon systems are well identified with an anti-phase of the annual cycle between the two hemispheres. Precipitation-related quantities (OLR and specific humidity), surface conditions [*i.e.*, mean sea level pressure (MSLP) and SST] and circulation fields related to moist convection systems show fundamental features of the global monsoon systems. After introducing eight QBO phases based on the leading two principal components of the zonal-mean zonal wind variations in the equatorial lower-stratosphere, the statistical significance of the composite difference in the precipitation and tropospheric circulation is evaluated for the opposite QBO phases. The composite differences show significant modulations in some regional monsoon systems, dominated by zonally asymmetric components, with the largest magnitudes for specific QBO-phases corresponding to traditional indices of the equatorial zonal-mean zonal wind at 20 and 50 hPa. Along the equator, significant QBO influence is characterized by the modulation of the Walker circulation over the western Pacific. In middle latitudes during boreal

summer, for a specific QBO-phase, statistically significant modulation of low-pressure cyclonic perturbation is obtained over the Northern-Hemisphere western Pacific Ocean associated with statistically significant features of heavier precipitation over the eastern side of the cyclonic perturbation and the opposite lighter precipitation over the western side. During boreal winter, similar significant low-pressure cyclonic perturbations were found over the Northern-Hemisphere eastern Pacific and Atlantic Oceans for specific phases.

Key words – Global monsoon systems, Equatorial QBO, Stratosphere-troposphere dynamical coupling, Stratospheric influence on the tropical troposphere.

1. Introduction

Monsoon is a periodic response of a large-scale circulation system in low and mid-latitudes to the annual cycle of solar forcing due to the revolution of the Earth around the Sun with a tilt of the rotation axis. The seasonal reversal of large-scale near-surface winds and heavy precipitation associated with the monsoon onset are important features of the monsoon (Krishnamurti *et al*., 2013; Chapter 5). Monsoons had traditionally been considered as being driven by continental-scale thermal contrast between lands and oceans (like large-scale sea breeze circulations). The primary driver of a global monsoon (GM) is the solar insolation and the specific features in the underlying surface, such as land-ocean distribution, topography and oceanic circulations, are mainly responsible for the differences among regional monsoon systems (Wang and Ding, 2008; Wang *et al*., 2017). In this century, a new perspective of GM systems emerged based on the fundamental recognition of the annual cycle response of global circulation systems with the important role of water circulation processes. There have been a series of research publications and review articles on GM systems in the last two decades or so [Chang *et al*. (Eds.), 2005, 2011, 2016, 2020].

The fundamental dynamics of the GM could stem from those of annually varying, zonally symmetric Hadley cells and Intertropical Convergence Zones (ITCZs), which have been investigated using hierarchical modeling approaches, including an aqua planet model, as recently reviewed by Geen *et al*. (2020). A better understanding of the GM requires the identification of its own dynamical characteristics and energy balances other than the annually migrating zonally symmetric ITCZs. Dynamical roles of the zonal asymmetries such as the land-ocean distribution, topography and oceanic circulations, influencing the GM, are essential to construct the observed characteristics of the large-scale tropical circulation and the GM systems.

As the variability of the GM systems on inter-annual time scales can have a profound societal and economic impact, it has been widely studied in association with a dominant surface dynamical variation known as El Niño Southern Oscillation (ENSO) (Krishnamurthy and Goswamy, 2000; Fan *et al*., 2017; Yun and Timmermann, 2018; Yu *et al*., 2021) and also in association with global warming situations by using hierarchical numerical models (Huang and Xie, 2015; He and Li, 2019; He *et al*., 2020). The impact of ENSO can be limited to any particular monsoon system and may depend upon timescales. Recently, Yu *et al*. (2021) showed that on the interannual (decadal) timescales, the Indian Summer Monsoon indicates a stronger (weaker) relationship with ENSO. On a longer time-scale, the response of regional monsoon systems under global warming can also be different with opposite signs. He *et al*. (2020) showed that the North American monsoon rainfall decreases in a warmer climate, in sharp contrast to the robust increase in Asian-African monsoon rainfall.

Furthermore, modulation of the annually periodic GM on interannual time scales is an interesting subject to another "external" forcing such as stratosphere-troposphere dynamical coupling [*e.g.*, the equatorial stratospheric Quasi-Biennial Oscillation (QBO)]. Stratosphere-troposphere dynamical coupling in the tropics through moist convective systems and their organizations has been studied under WCRP/SPARCSATIO-TCS (Stratospheric and Tropospheric Influences on Tropical Convective Systems) activity (Hitchcock *et al*., 2019; Yoden *et al*., 2020). Interest in the downward influence of the stratosphere on tropical convection has grown rapidly since the discovery of the pronounced influence of the stratospheric QBO on the Madden Julian Oscillation (MJO) in the equatorial region by Yoo and Son (2016), as reviewed by Martin *et al*. (2021), although the investigations of stratospheric influences on the tropical and subtropical upper troposphere and lower stratosphere and also on tropical convective systems have a longer history as reviewed by Hitchman *et al*. (2021) and Haynes *et al*. (2021).

The influence of the stratospheric QBO on tropospheric moist convection and its organizations into meso-scale to planetary-scale systems have been studied for sub-seasonal to inter-annual time-scale variations in the tropics, such as the MJO and the ENSO. In addition, there could be the QBO modulation of the periodic annual cycle of the GM systems. In this study, after describing fundamental climatological characteristics of the GM for the neutral ENSO periods, a statistical significance test on the influence of the equatorial stratospheric QBO on the GM systems is made in the wet and dry seasons of monsoons, or two solstice seasons in June, July and August (JJA) and December, January and

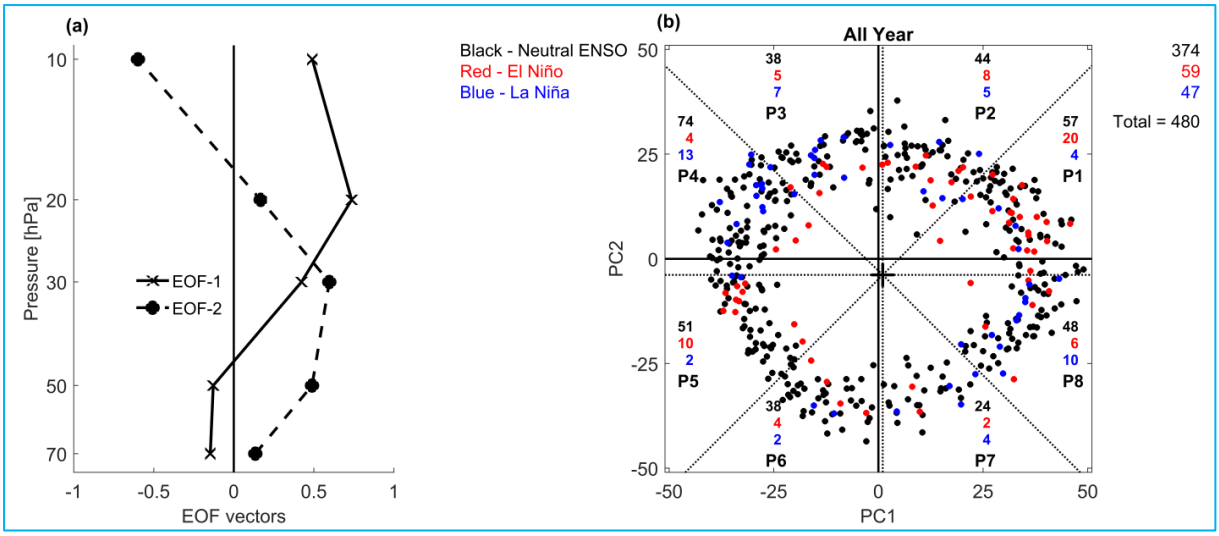

Figs. 1(a&b). EOF analysis of the zonal-mean zonal wind anomalies [*U'*] in the equatorial lower stratosphere. (a) Vertical profiles of EOF1 and EOF2, which explain 59.7% and 34.9% of the total variance, respectively and (b) Scatter plot of *PC*1 and *PC*2 for 40 years. Numbers of months for neutral ENSO (black), El Niño (red) and La Niña (blue) are given for the total period at the top right corner and for eight QBO phases, Phase 1 (P1) to Phase 8 (P8)

February (DJF), by using monthly-mean ERA-Interim reanalysis and some other datasets for 40 years.

2. Data and methodology

2.1. *Data and focusing on the neutral ENSO periods*

Monthly-mean ERA-Interim reanalysis data for 40 years from 1979 to 2018 are used for the analysis, same as described in detail by Kumar *et al*. (2022).We use the horizontal distributions of zonal and meridional winds (*U*, *V*), vertical wind *W*, temperature *T* and mean sea-level pressure *MSLP* for the circulation fields and specific humidity *q* in relation to precipitation. Monthly-mean data of NCAR GPCC (2020) precipitation *P* and NOAA Outgoing Longwave Radiation *OLR* (Lee and NOAA CDR Program, 2018) are also used as rainfall-related quantities.

As in Kumar *et al*. (2022), The Hadley Centre Sea Surface Temperature *SST* dataset is used to calculate the monthly Niño 3.4 index for ENSO variations. In this study, the 480 months of all-year data are divided into three phases of ENSO by introducing the threshold values, ± 1 K from the climatological annual cycle, to yield 374 neutral months, 59 El Niño months and 47 La Niña months [Fig. 1(b)]. We analyze the neutral periods focusing on the general features without extreme conditions of El Niño or La Niña. Note that the joint influence of the stratospheric QBO and the tropospheric ENSO in the tropics was studied by Kumar *et al*. (2022) with a similar composite difference analysis.

This study explores both zonal mean and zonally asymmetric features during the boreal summer season, JJA, which is the wet monsoon season in the Northern Hemisphere (NH), separately from the austral summer season, DJF, which is the wet monsoon season in the Southern Hemisphere (SH). Composite differences between the two seasons, JJA-DJF, give the general features of the GM systems in a wide perspective of circulation and precipitation fields.

2.2. *Eight QBO phases based on a principal component analysis*

We apply the composite difference analysis (Kumar *et al*., 2022) that uses the QBO-phase angles based on the leading two principal components of the EOF analysis for the deseasonalized zonal-mean zonal wind variations [*U'*] in the equatorial lower-stratosphere introduced by Wallace *et al*. (1993). Hereafter a single prime superscript on any variable, *X'*, represents its deviation from the mean climatological annual cycle for the 40-year period, *i.e*., a deseasonalized anomaly. Fig. 1(a) shows the vertical profiles of EOF1 and EOF2 for [*U'*], which explain 59.7% and 34.9% of the total variance in the lower stratosphere (10 to 70 hPa) respectively. The scatter plot of the leading two principal components, *PC1*(*t*) and *PC2*(*t*),is shown in Fig. 1(b) for the 480 months with the distinction of neutral ENSO (black), El Niño (red) and La Niña (blue) periods.

The QBO-phase angle θ is defined as the arctangent of [*PC2*(*t*) / *PC1*(*t*)] after shifting the origin to the centroid

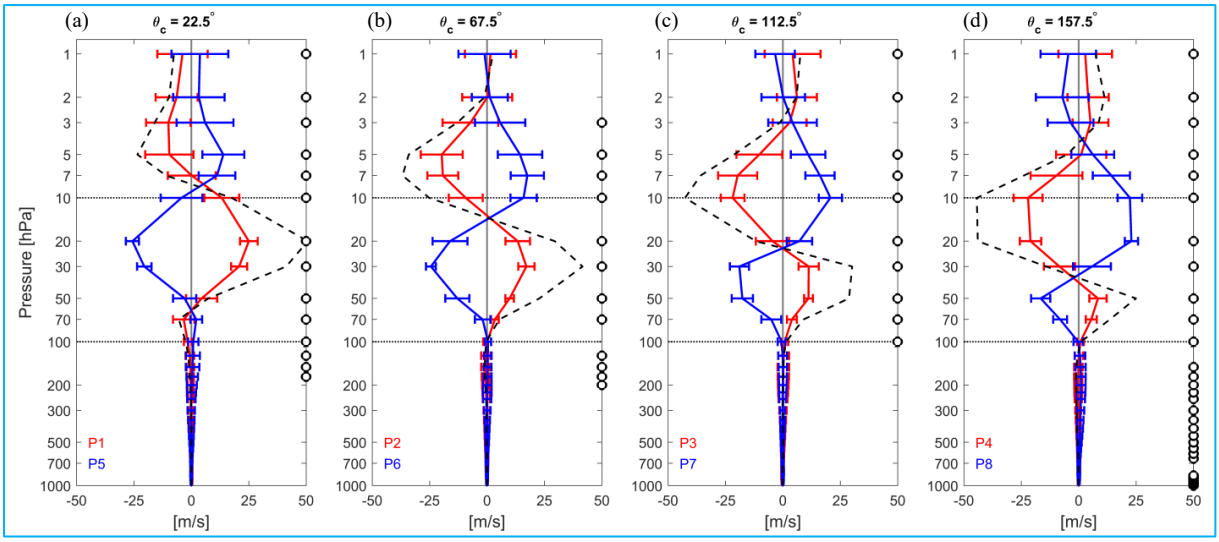

Figs. 2(a-d). Vertical profile of the composite mean (solid line) and ± one standard deviation (horizontal bar) of the deseasonalized zonal-mean zonal wind anomalies [U'] on the equator for eight QBO phases, (a) P1/P5 to (d) P4/P8. P1~P4 in red line and P5~P8 in blue line, together with the composite difference between them (*e.g.*, P1−P5) in black dashed line. Circles on the right-hand side of each frame indicate a statistically significant (> 90%) composite difference at the corresponding pressure levels

of all data points (shown as a + marker). Where, eight QBO phases are introduced with 45-degree increments ($\Delta\theta = 45°$) for each to evaluate the statistical significance of the difference of composite means with opposite QBO phases. In Kumar *et al*. (2022), a wider $\Delta\theta$ of 120° was chosen and the central angle θ_c was swept for every 1° by showing insensitive results of the statistically significant features in composite differences between opposite phases. This would be another approach, like the division into eight phases of the MJO based on the angle on *PC1*(t)-*PC2*(t) phase plane, such as the real-time multivariate MJO index, *RMM* (Wheeler and Hendon, 2004).

2.3. *Statistical significance of composite differences with opposite QBO phases*

Figs. 2(a-d) show the vertical profile of the composite mean (solid line) and ± one standard deviation (horizontal bar) of the deseasonalized zonal-mean zonal wind [U'] on the equator for eight QBO phases, from (a) for Phase 1 (red) and Phase 5 (blue) to (d) for Phase 4 (red) and Phase 8 (blue). A black dashed line in each plot also denotes the composite difference between opposite phases of the QBO (*i.e.*, red line-blue line).The composite profile shows a clear QBO cycle in the middle and lower stratosphere with a node between these layers and most of the composite differences with opposite QBO phases are statistically significant except for the upper stratosphere in (b), *i.e.*, Phase 2 - Phase 6 at 1 and 2 hPa. In this study, the statistical significance of the composite difference is evaluated using a two-sided Student's *t*-test at 90% confidence level, assuming two independent samples in each group. The composite differences are also statistically significant around the tropopause in (a) and (b) and throughout the troposphere in (d), even though the difference is very small if compared with the signals in the lower stratosphere.

3. Results

3.1. *Climatology of the GM for the neutral ENSO periods*

Figs. 3(a-d) show the climatology of the GM systems for the neutral ENSO periods viewed in longitude-latitude sections of precipitation P and horizontal winds (U, V) in the lower troposphere at 850 hPa in the 3rdcolumn, together with the zonal mean [U] (solid line) and [V] (dashed line) in the 1st column and the zonal mean precipitation [P] in the 2nd column. The 1st row is for the annual mean, the 2nd row is for JJA mean, the 3rd row is for DJF mean and the 4th row is for the composite difference, JJA-DJF. Annually averaged P shows clear features of the Pacific and Atlantic ITCZs around 7° N, which contribute to the peak of [P] in the 2nd column. It also shows the features of the South Pacific Convergence Zone (SPCZ) and Indian Ocean ITCZ in the SH with a broader meridional extent. Seasonal variations are clear in the lower tropospheric wind vectors $\boldsymbol{U} = (U, V)$ in the 2nd and 3rdrows as the dominance of anticyclonic circulations

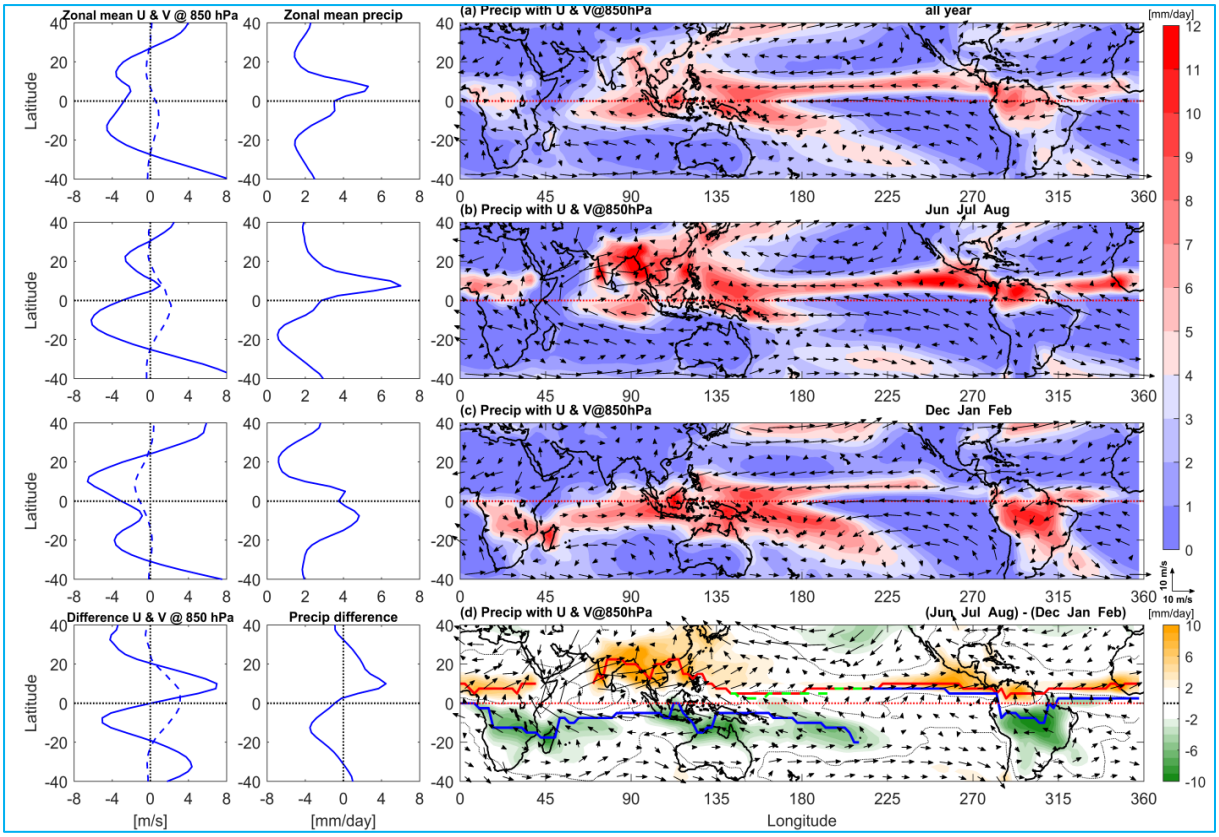

Figs. 3(a-d). Climatology of precipitation P and horizontal winds (U, V) at 850 hPa for 40 years (1979-2018) during the neutral ENSO periods from 40° S to 40° N. The 1st column represents the zonal mean [U] (solid line) and [V] (dashed line), the 2nd column the zonal mean P *and* the 3rd column the longitude-latitude section of P in color tones with (U, V) vectors at 850 hPa in black arrows. (a) annual mean, (b) JJA mean, (c) DJF mean and (d) composite difference of JJA-DJF. In the composite difference panel (d), the color tones are shown if the magnitude of rainfall exceeds 2 mm/day

over oceans in summer (*i.e.*, over the NH Pacific and Atlantic Oceans in JJA, whereas over the SH Pacific, Atlantic and Indian Oceans in DJF).

Seasonal variations or the differences between wet and dry monsoon seasons are clearly seen in the composite difference of Pin the 4th row of Fig. 3(d). All six monsoon systems over the globe, including Asian, North African, North American, Australian, South African and South American Monsoons are clearly seen by the golden (in the NH) and green (in the SH) colors in the composite difference patterns (JJA-DJF) in Fig. 3(d). The position of ICTZ is determined on the basis of maximum rainfall intensity if it exceeds 2 mm/day and shown with a red (blue) line for boreal summer season JJA (austral summer season DJF) as illustrated in Wang *et al*. (2021). Some prominent regional monsoon systems could be recognized, such as South Asian, South-East Asian and East Asian (plus Western North Pacific Ocean) Monsoons in the NH and Australian and Maritime Continent Monsoons in the SH. This figure provides similar features between the two hemispheres with an anti-phase of the annual cycle, as described in *e.g.*, Geen *et al*. (2020). Similar plots of precipitation patterns with the GM divergent circulation can be found in Wang *et al*. (2017). Annual-cycle features of cross-equatorial flows in the lower troposphere are also well captured in the composite difference map; over the western Indian Ocean known as Somali Jet Stream, over the Maritime Continent and over the South American Continent. Wang and Ding (2008) made a multivariable EOF analysis on the annual march of climatological monthly mean precipitation and horizontal winds at 850 hPa and obtained a solstitial mode as the 1st mode of the annual cycle that accounts for 71% of the total variance. The spatial patterns of the solstitial mode [their Fig. 3(a)] show similar horizontal patterns of P and $\boldsymbol{U}$ at 850 hPa as obtained bythe composite difference analysis in this study [Fig. 3(d) (right)].

The zonal-mean horizontal winds [U] and [V] and precipitation [P] also show large annual cycles, or variations between wet and dry monsoons, with a half-

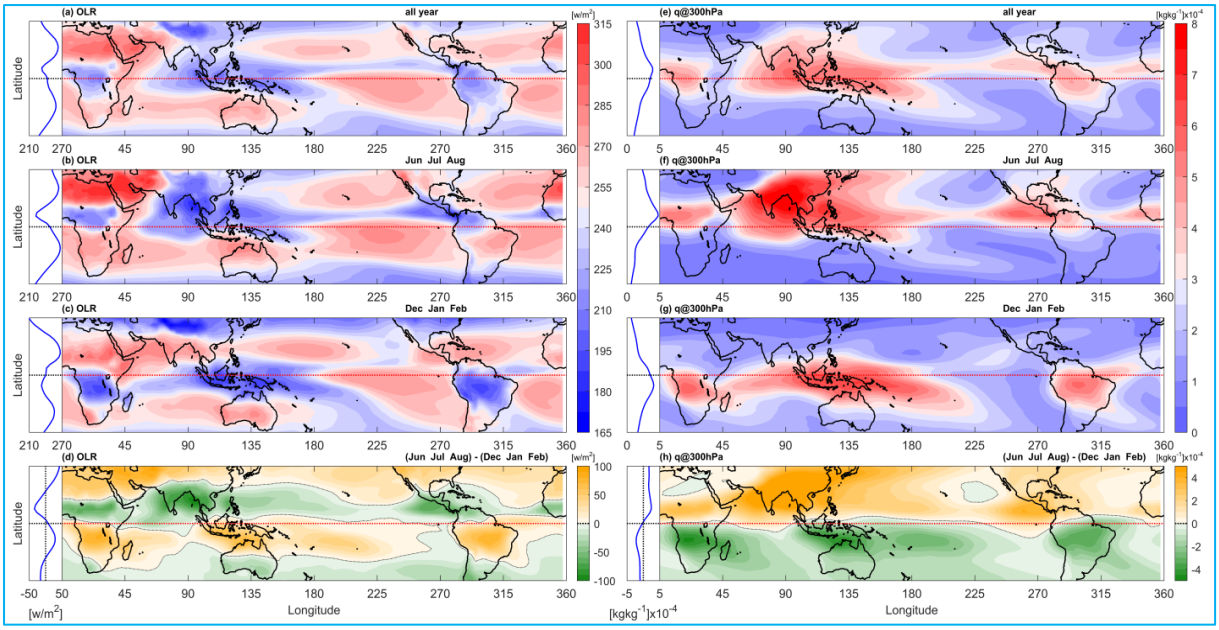

Figs. 4(a-h). Climatology of precipitation-related quantities *OLR* [left panels from (a) to (d)] and specific humidity *q* at 300 hPa [right panels from (e) to (h)] for 40 years (1979-2018) during the neutral ENSO periods from 40° S to 40° N. The zonal mean profile of each quantity is shown with an adjacent blue line plot on the left-hand side. In each group, (1st row) annual mean, (2nd row) JJA mean, (3rd row) DJF mean and (4th row) composite difference, JJA-DJF

year time difference between the NH and the SH. The annual cycles of the zonal mean quantities deviated from the annual mean are significant and well captured in the composite difference (JJA-DJF) in the 4th row. The zonal-mean [*U*] and [*P*] show nearly anti-symmetric profiles with respect to the equator, whereas the zonal-mean [*V*] is nearly symmetric. These are another way of describing and recognizing the annual cycle responses with a half-year time difference between the two hemispheres.

Figs. 4(a-h) show the climatology of precipitation-related quantities, *OLR* in the left panels and specific humidity *q* at 300 hPa in the right panels [four rows for each group as in Figs. 3(a-d)] for the neutral ENSO periods. Horizontal distributions of *OLR* show smoother and larger-scale patterns than the precipitation field. The composite difference (JJA-DJF) field in the 4th row shows negative peaks of *OLR* corresponding to deep convective systems associated with Asian, North American and North African Monsoons in the NH, whereas positive ones with a half-year difference associated with Maritime Continent/ Australian, South American and South African Monsoons [Fig. 4(d)]. The composite difference of *q* at 300 hPa shows much smoother distribution patterns with nearly anti-symmetric profiles with respect to the equator as also seen in the zonal-mean plot [associated line plot with Fig. 4(h)]. Local minima of the composite difference are recognized in the both-hemisphere subtropics in the eastern part of the Pacific and Atlantic Oceans and the SH Indian Oceans.

Figs. 5(a-h) show the climatology of surface conditions, *MSLP* together with (*U*, *V*) at 850 hPa in the left panels and *SST* in the right panels [four rows for each group as in Figs. 3(a-d)] for the neutral ENSO periods. Horizontal distributions of *MSLP* show the strongest monsoon depressions over South Asia (and Middle East) in JJA and over Australia and Maritime Continent in DJF. In the summer hemisphere, anticyclones and associated lower-tropospheric circulations over oceans are prominent, *i.e.*, over the NH Pacific and Atlantic Oceans in JJA, whereas over the SH eastern Pacific, Atlantic and Indian Oceans in DJF. Along the equator, *MSLP* is relatively low over the Maritime Continent and the western Pacific Ocean with annual variations, together with the lower-tropospheric easterlies constituting the Walker circulation. The composite difference of *MSLP* shows anti-symmetric features of the GM systems with respect to the equator, more clearly in the zonal-mean plot [associated line plot with Fig. 5(d)]. The contrast between lands and oceans is clearer in the NH. The highest *SST* is seen in the eastern Indian Ocean to the western Pacific along the equator with small annual-cycle variations. The composite difference of *SST* between JJA-DJF shows anti-symmetric distributions with respect to the equator (warmer in the summer hemisphere mid-latitudes) with a rather small zonal dependence; its meridional gradient is relatively large on the western side of the oceans.

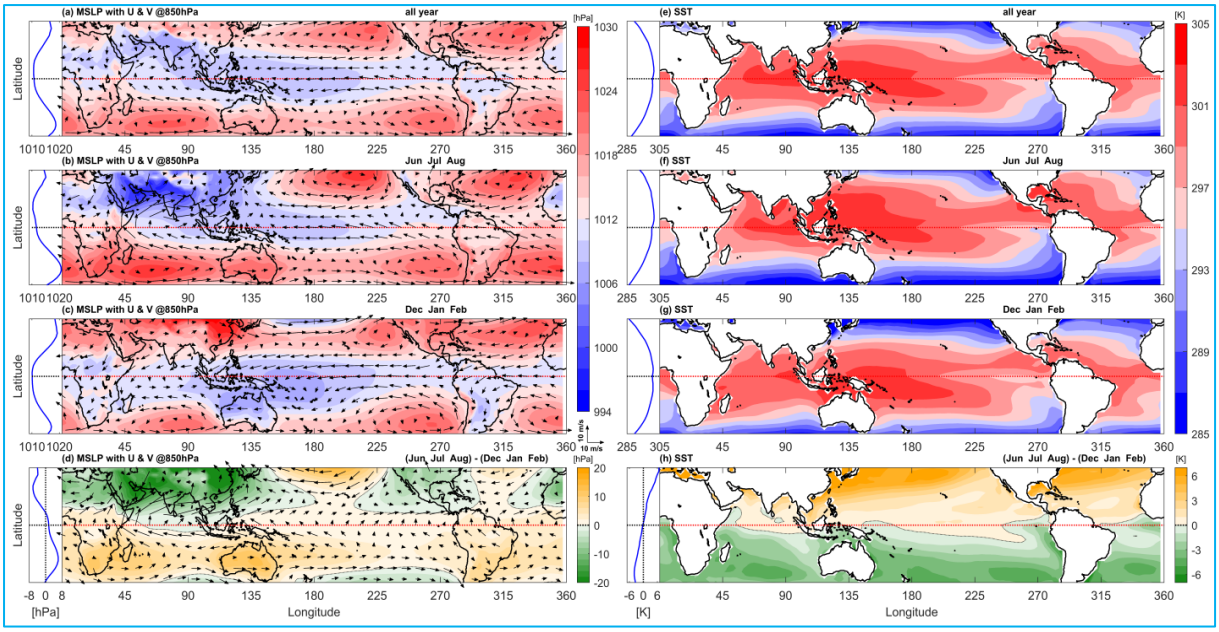

Figs. 5(a-h). As in Figs. 4(a-h) but for *MSLP* with (*U*, *V*) vectors at 850 hPa [left panels from (a) to (d)] and *SST* [right panels from (e) to (h)]

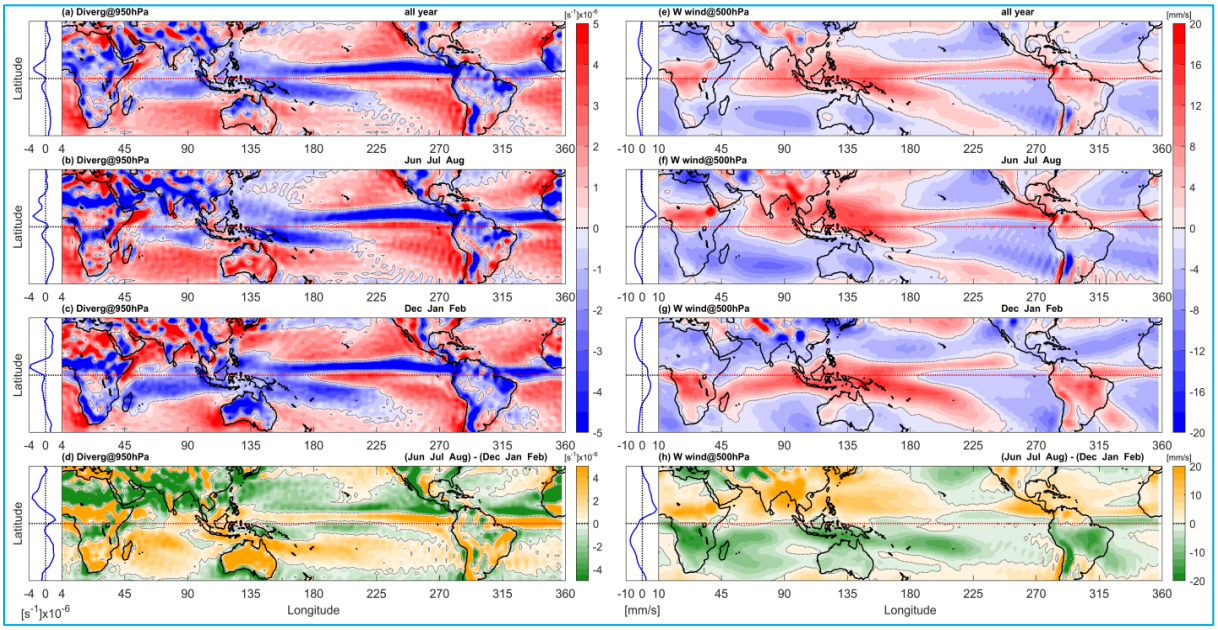

Figs. 6(a-h). As in Figs. 4(a-h) but for the horizontal divergence of (*U*, *V*) at 950 hPa [left panels from (a) to (d)] and vertical wind *W* at 500 hPa [right panels from (e) to (h)]

Figs. 6(a-h) show the climatology of circulation fields associated with moist convection systems, that is, the divergence of horizontal wind, div ***U***, in the planetary boundary layer at 950 hPa in the left panels and mid-tropospheric vertical wind, *W*, at 500 hPa in the right panels [four rows for each group as in Figs. 3(a-d)] for the neutral ENSO periods. The annual-mean and seasonal-mean plots in both groups show a convergence field in the boundary layer and mid-tropospheric upward motion associated with the Pacific and Atlantic ITCZs in the NH and the SPCZ and Indian Ocean ITCZ in the SH as identified in the precipitation *P* field shown in Figs. 3(a-d).

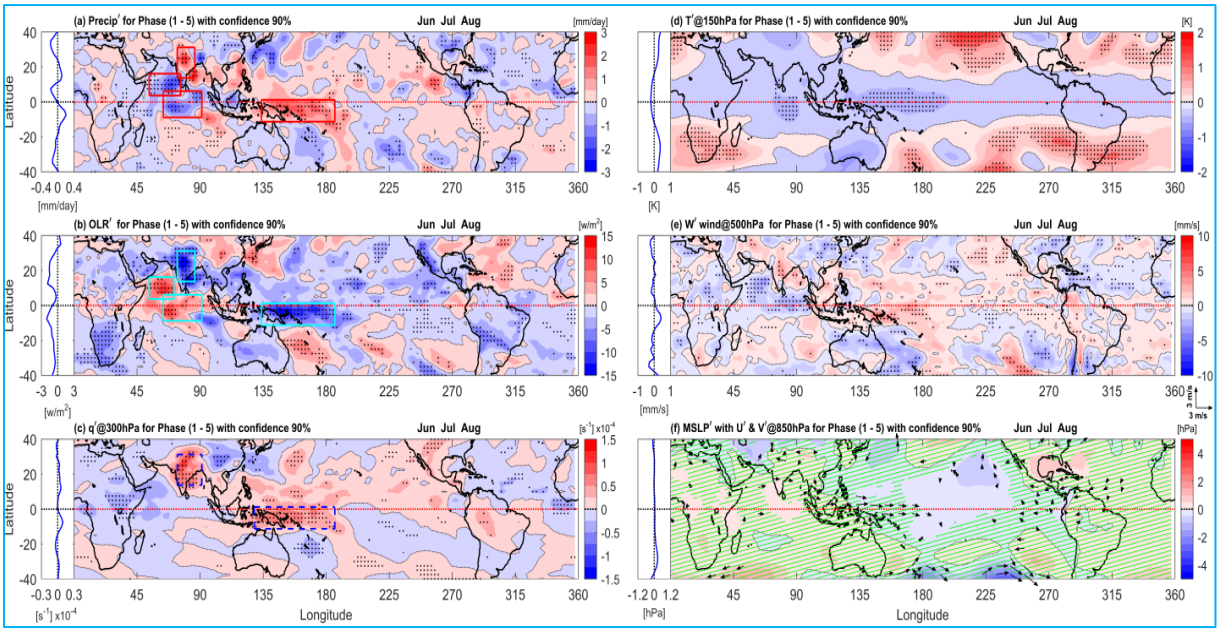

Figs. 7(a-f). Composite differences of six quantities between opposite QBO phases for Phase 1- Phase 5 during boreal summer, JJA. (Left panels) longitude-latitude sections of precipitation and its related quantities for (a) precipitation *P*, (b) *OLR* and (c) specific humidity *q* at 300 hPa, together with the zonal mean profile of the adjacent blue line plot on the left-hand side. (Right panels) longitude-latitude sections of circulation fields for (d) temperature *T*at 150 hPa, (e) *W* at 500 hPa and (f) *MSLP* with (*U*, *V*) vectors at 850 hPa. In (a) to (e), shadings with black dots show the areas where the statistical significance of composite difference exceeds 90% confidence level, whereas in (f), green hatchings show regions with less than 90% confidence level of the statistical significance and (*U*, *V*) vectors are plotted only if either component exceeds 90% confidence level. In longitude-latitude sections in the left panels, rectangular boxes show some highly significant regions of precipitation and its related quantities

Annual meridional migration of ITCZs is identified as a pair of negative and positive zonally elongated stripes in the composite difference plots of div ***U*** and *W*, as clearly seen for the Pacific and Atlantic ITCZs in the NH. The composite difference of the mid-tropospheric vertical wind shows similar features as that of precipitation in Figs.3(a-d) for regional monsoon systems; large magnitudes and wide areas of Asian (and Western North Pacific), North American and North African Monsoons in the NH and those of Australian (and Maritime Continent), South American and South African Monsoons in the SH. On the other hand, the convergence field in the boundary layer also shows smaller-scale features associated with near-surface winds and surface topography, such as the mountain ranges of the Western Ghats in India, the Sierra Madre in Mexico and the Andes in South America.

3.2. *Significant composite differences of opposite QBO phases*

Modulations of the GM systems by the equatorial stratospheric QBO are studied by the composite difference analysis as described in Section 2 for two solstice seasons, JJA and DJF, boreal and austral summer (or, a wet monsoon season in the NH and the SH), respectively. As for the QBO phases, we focus on two pairs of Phase 1-Phase 5 and Phase 4-Phase 8, because in the former phases the zonal-mean [*U'*] has the largest difference at 20 hPa, whereas in the latter phases it has a local maximum at 50 hPa as shown in Figs. 2(a-d) [Fig. 20 in Hitchman *et al*. (2021)]. That is, in Phase 1 (Phase 5), [*U'*] is westerly (easterly) maximum at 20 hPa, whereas in Phase 4 (Phase 8), [*U'*] is westerly (easterly) local maximum at 50 hPa with an opposite-sign large-magnitude [*U'*] at 10 and 20 hPa. These phases at a specific level have been frequently used in previous data-analysis studies to make two groups with opposite QBO phases. The same physical quantities [GPCC *P*; NOAA *OLR*; ERA-Interim (*U*, *V*, *W*), *MSLP* and *q*] as used in Section 3.1 for the climatological description are analyzed. To avoid monthly intra-seasonal variability within the cluster of the two seasons, JJA and DJF, deseasonalized anomalies of each quantity are used for the composite difference analysis (*i.e.*, deviations from the climatological annual cycle) only for the neutral ENSO periods, excluding the influences of El Niño or La Niña.

Figs. 7(a-f) and 8(a-f) show composite differences between the opposite QBO phases of Phase 1 - Phase 5 and Phase 4 - Phase 8, respectively, during boreal

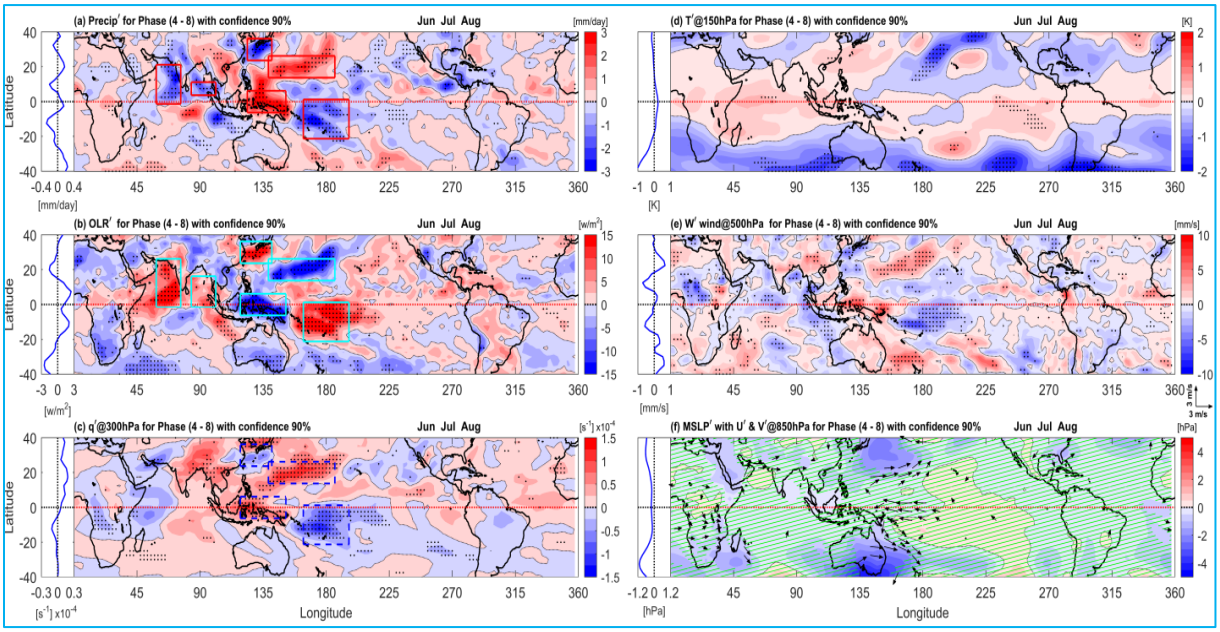

Figs. 8(a-f). As in Figs. 7(a-f) but for Phase 4-Phase 8 (during boreal summer, JJA)

summer, JJA. The left panels are the zonal-mean profiles and longitude-latitude sections of precipitation, *P'* (1st row) and its relevant physical quantities of *OLR'* (2nd row) and *q'* at 300 hPa (3rd row), whereas the right panels are those of circulation fields, such as temperature, *T'* around the tropopause at 150 hPa (1st row), *W'* at 500 hPa (2nd row) and *MSLP'* with (*U'*, *V'*) vectors at 850 hPa (3rd row). The rectangular boxes in the left panels show the major statistically-significant areas of precipitation and its relevant quantities.

It is obvious that zonally asymmetric components dominate and the obtained zonal-mean features are just a result of the averaging process with little relevance to zonally elongated features, such as Pacific or Atlantic ITCZ stripes seen in the climatology. Composite differences of each quantity show statistically significant modulations of regional monsoon systems with the largest magnitudes for Phase 4-Phase 8 [Figs. 8(a-f)], the second ones for Phase 1-Phase 5 [Figs. 7(a-f)] and smaller magnitudes for the other two pairs (not shown). Significant large-magnitude features are observed over the Maritime Continent and western Pacific along the equator and Asian monsoon regions, including in adjacent the western Pacific and Indian Oceans. Note the positive spatial correlations between *P'* and *q'* at 300 hPa over the regions, with negative correlations with *OLR'* and also some positive correlations with *W'* at 500 hPa. All these correlations are supportive of heavier precipitation with humid air in the upper troposphere, associated with more intensive moist convection with lower *OLR'* and stronger upward motion in the middle troposphere. Dipole patterns of these quantities over the Maritime Continent and western Pacific along the equator suggest the modulation of Walker circulation accompanied by the modulations of zonal winds in the lower troposphere at 850 hPa, under a QBO-phase dependence, as shown in Figs. 7(a-f) and 8(a-f). Along the equator over the western Pacific, significant QBO modulations of the precipitation-related quantities are associated with *T'* difference around the tropopause at 150 hPa for Phase 1-Phase 5 [Fig. 7 (d)], whenever the equatorial QBO wind has a maximum at 20 hPa.

In middle latitudes in the plots for Phase 4-Phase 8 [Figs. 8(a-f)], statistically significant composite differences are seen in *MSLP'* together with lower tropospheric horizontal winds in both hemispheres over the western Pacific. Upward motions *W'* in the middle troposphere are also significant over the eastern side of the low-pressure cyclonic circulations. In the NH, heavier precipitation features of *P'*, *OLR'* and *q'* are also statistically significant over the eastern side of the low-pressure system, where as lighter precipitation features of *P'* and *OLR'* are significant over the western side of the low-pressure system (south of Japan).

Similarly, Figs. 9(a-f) and 10(a-f) show composite differences between the opposite QBO phases of Phase 1-Phase 5 and Phase 4-Phase 8, respectively, during austral summer, DJF. In the plots for Phase 1-Phase 5 [Figs. 9(a-f)], statistically significant regional features with large magnitude are found as the modulation of Walker

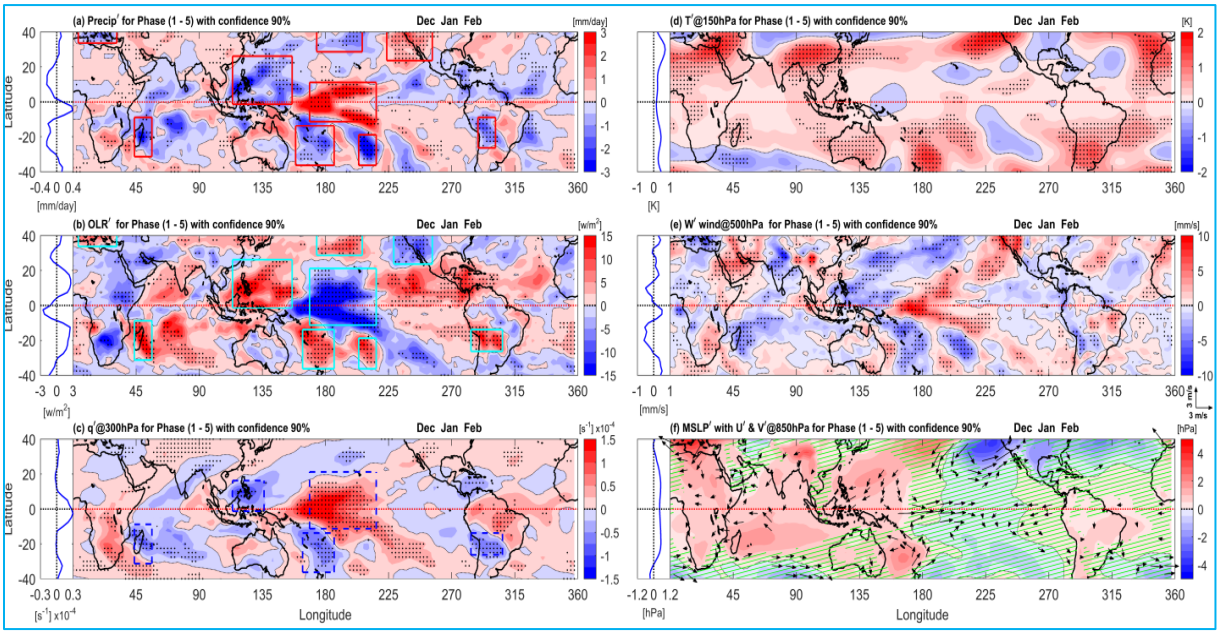

Figs. 9(a-f). As in Figs. 7(a-f) but for austral summer, DJF (for Phase 1 - Phase 5)

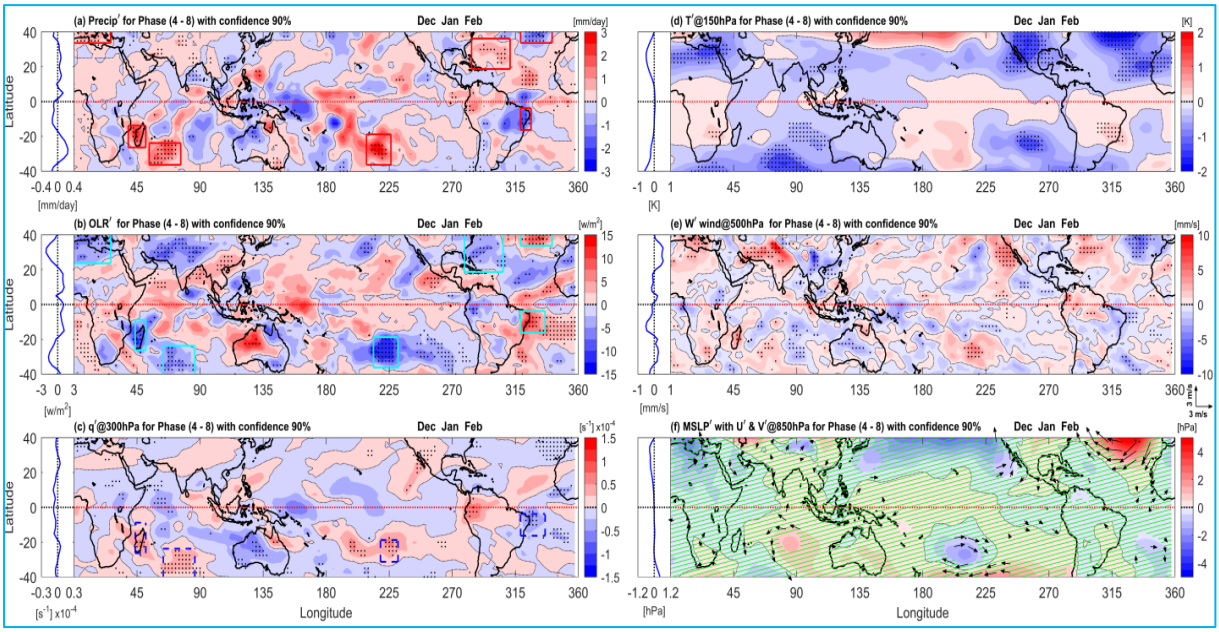

Figs. 10(a-f). As in Figs. 7(a-f) but for Phase 4-Phase 8 during austral summer, DJF

circulation over the western Pacific Ocean along the equator. Note that the positive spatial correlations among *P', q'* at 300 hPa and *W'* at 500 hPa over the regions, with negative correlations with *OLR'*, together with eastward wind *U'* at 850 hPa show significant QBO influence on tropical convection systems in these phases between Phase 1-Phase 5 with the largest QBO-wind difference at 20 hPa. All these correlations are supportive of heavier precipitation associated with more intensive moist convection systems over the western Pacific in Phase 1.

In middle latitudes in the plots for Phase 1-Phase 5 [Figs. 9(a-f)], statistically significant composite differences are seen as a low-pressure perturbation in

MSLP' together with lower-tropospheric cyclonic horizontal winds in the NH over the eastern Pacific Ocean. Upward motions *W'* in the middle troposphere are also significant over the eastern side of the low-pressure cyclonic circulations, together with heavier precipitation features of *P'*, *OLR'* and *q'* over the eastern side of the low-pressure system and lighter precipitation features over the western side. On the other hand, in the plots for Phase 4-Phase 8 [Figs. 10(a-f)], statistically significant composite differences are seen as a high-pressure feature in *MSLP'* over the NH Atlantic Ocean. Downward motions *W'* in the middle troposphere are also significant over the eastern side of the high-pressure anticyclonic circulations, together with lighter precipitation features of *P'*, *OLR'* and *q'* over the eastern side of the high-pressure system and heavier precipitation features over the western side. In other words, this is a low-pressure cyclonic circulation with heavier precipitation features over the eastern side seen in Phase 8-Phase 4 composite difference *i.e*., the opposite sign plots of Figs. 10(a-f), which is a similar feature of composite difference over eastern Pacific for the same boreal winter, DJF, as seen for Phase 1-Phase 5. The QBO modulation of *T'* around the tropopause for Phase 1- Phase 5 is significantly positive in association with a low-pressure cyclonic circulation over the eastern Pacific Ocean [Figs. 9(d&f)], whereas that for Phase 4-Phase 8 is significantly negative in association with a high-pressure anticyclonic circulation over the Atlantic Ocean [Figs. 10(d&f)]. These composite differences of temperature anomalies around the subtropical tropopause are the same sign as the zonal-mean temperature anomaly associated with the equatorial QBO and significantly large and positive in a synoptic scale; over the eastern Pacific Ocean for Phase 1-Phase 5 and over the Atlantic Ocean for Phase 8-Phase 4.

4. Discussion

Long enough observation data are desirable to obtain a statistically significant result on the influences of the equatorial QBO on tropical deep convection and its organizations up to large-scale circulations. Among a numerous number of previous studies on observational data analyses, some challenging studies in the early years include Collimore *et al*. (1998) who analyzed a 12-year record of OLR for 1975-87 to test the proposition that the QBO modulates deep tropical convection and Collimore *et al*. (2003) who analyzed 23-year OLR record and 17-year record of the highly reflective cloud (HRC) index of a gridded, monthly count of cloud clusters. About a decade later, Liess and Geller (2012) used a cluster analysis of 21.5-year data from International Satellite Cloud Climatology Project (ISCCP) tropical weather states to identify tropical deep convection and cirrus clouds, as well as 32.25-year precipitation data as proxies for deep convection. Recently, Lee *et al*. (2019) used five metrics representing tropical convection over 32 years (1979-2010): (*i*) GPCP precipitation, (*ii*) NOAA OLR, (*iii*) convective available potential energy (CAPE), (*iv*) deep convective heating rate and (*v*) convective cloud top pressure, where (*iii*)-(*v*) are calculated from reanalysis data, to investigate differences in the tropical convective activities at the opposite phases of the QBO. As data volume growth has been slow, we could use 40-year data in this study (a couple of times longer data length than the earlier studies), by taking a similar strategy to use independent observation data such as GPCC precipitation and NOAA OLR, as well as ERA-Interim reanalysis data.

Another point to overcome the limited data length in this study is the careful treatment of possible contamination of the ENSO effect in the diagnosis of the QBO influence. As considered in some previous studies, we use only the neutral ENSO periods focusing on the general feature without extreme conditions of El Niño or La Niña, even though it further limits the total length of data to be analyzed. On the other hand, the joint influence of the stratospheric QBO and the tropical tropospheric ENSO is an interesting subject besides to this work and the results of composite difference analysis were reported by Kumar *et al*. (2022).

As described in Section 3.2., in middle latitudes, a statistically significant negative composite difference is found during boreal summer for Phase 4-Phase 8 in MSLP together with lower tropospheric cyclonic circulation over the NH western Pacific Ocean, whereas similar significant composite differences are obtained during boreal winter for Phase 1-Phase 5 over the NH eastern Pacific Ocean and for Phase 8-Phase 4 over the NH Atlantic Ocean. The difference in the observed season, boreal summer or winter, in these significant remote linkages would give good examples for investigating the pathways of communication from the equatorial QBO to the lower troposphere through the extra tropical (*i.e.*, stratospheric), subtropical, or tropical pathway, as discussed in Haynes *et al*. (2021). At least the stratospheric pathway should be excluded in the boreal summer case.

5. Conclusions

Monthly-mean data from ERA-Interim reanalysis, GPCC precipitation, NOAA OLR and Hadley Centre SST for 40 years from 1979 to 2018were analyzed to reveal the modulation of global monsoon systems by the equatorial QBO, focusing only on the neutral ENSO periods (in total 374 months out of 480 months).

First, climatology of the global monsoon systems was viewed at longitude-latitude distributions of

precipitation and horizontal winds in the lower troposphere [as shown in Figs. 3(a-d)] for the annual mean and two solstice seasons of JJA and DJF, for the NH and the SH wet monsoon seasons, respectively, together with the differences of composite maps for the two seasons, JJA-DJF. In addition to the annual meridional migration of the Pacific and Atlantic ITCZs in the NH and the seasonal variations of the broader SPCZ and Indian Ocean ITCZ in the SH, several regional monsoon systems were well identified with an anti-phase of the annual cycle between the two hemispheres, including Asian Monsoons, North American Monsoon and North African Monsoon in the NH and Australian/Maritime Continent Monsoon, South American Monsoon and South African Monsoon in the SH. Annual-cycle features of cross-equatorial flows in the lower troposphere were also well captured in the composite difference map, over the western Indian Ocean (known as Somali Jet Stream), Maritime Continent and South American Continent.

Climatology of OLR and specific humidity in the upper troposphere shows larger-scale patterns smoother than the precipitation field [Figs. 4(a-h)]. Horizontal distribution of MSLP shows the strongest monsoon depressions over South Asia (and Middle East) in JJA and over Australia and the Maritime Continent in DJF [Figs. 5(a-d)]. In the summer hemisphere, anticyclones and associated lower tropospheric circulations over oceans are prominent; *i.e*., over the NH Pacific and Atlantic Oceans in JJA, whereas over the SH eastern Pacific, Atlantic and Indian Oceans in DJF. Along the equator, MSLP is relatively low over the Maritime Continent and the western Pacific Ocean with annual variations, together with the lower-tropospheric easterlies constituting the Walker circulation. Climatology of circulation fields associated with moist convection systems, that is, the divergence of horizontal wind in the planetary boundary layer and mid-tropospheric vertical wind [Figs. 6(a-h)], also show consistent features with the mean plots and the composite difference for the precipitation, as well as the convergence field in the boundary layer with smaller-scale features associated with near-surface winds and surface topography.

To investigate the modulation of the global monsoon systems by the equatorial QBO, a composite difference analysis was performed by using a QBO-phase angle based on the leading two principal components of the EOF analysis for the zonal-mean zonal wind variations in the equatorial lower-stratosphere. Eight QBO phases (45 degrees each) were introduced to evaluate the statistical significance of the differences in composite means of precipitation and tropospheric circulations between opposite QBO phases. The equatorial QBO signal in the zonal-mean zonal wind has the largest difference for Phase 1 (westerly)-Phase 5(easterly) at 20 hPa, whereas for Phase 4 (westerly)-Phase 8(easterly) at 50 hPa with opposite-sign larger-magnitude differences at 10 and 20 hPa levels [Figs. 2(a&d)].

The composite differences of each quantity show statistically significant modulations of some regional monsoon features, dominated by zonally a symmetric components, with the largest magnitudes for Phase 4-Phase 8 [Figs. 8(a-f)] and second ones for Phase 1-Phase 5 [Figs. 7(a-f)] during boreal summer JJA, whereas with the largest magnitudes for Phase 1-Phase 5 [Figs. 9(a-f)] during boreal winter DJF. Large significant modulations during boreal summer are observed mostly in the Asian monsoon systems such as South Asian (plus Indian Ocean), South-East Asian and East Asian (plus Western North Pacific Ocean) Monsoons for Phase 4-Phase 8 and some of these for Phase 1-Phase 5. Along the equator, for Phase 4-Phase 8 [Figs. 8(a-f)], a significant QBO modulation in the troposphere is characterized by the enhancement of the Walker circulation over the western Pacific Ocean that leads to more precipitation over the Maritime Continent and consequently less over the Western Pacific Ocean. Also, less precipitation is observed in the Arabian Sea of the South Asian Monsoon region.

In middle latitudes during boreal summer, for Phase 4-Phase 8 [Figs. 8(a-f)], a statistically significant negative composite difference is obtained in MSLP together with lower tropospheric cyclonic circulation over the NH western Pacific Ocean. Over the eastern side of the low-pressure cyclonic circulation, upward motions are also significant in the middle troposphere, together with statistically significant features of heavier precipitation including OLR and specific humidity, whereas the opposite lighter precipitation features are significant over the western side of the low-pressure system (south of Japan). During boreal winter, similar significant low-pressure cyclonic circulations are also found over the NH eastern Pacific Ocean for Phase 1-Phase 5 [Figs. 9(a-f)] and over the NH Atlantic Ocean for Phase 8-Phase 4 (as negative-sign plots of Figs. 10(a-f) for Phase 4-Phase 8), together with statistically significant features of heavier precipitation including mid-tropospheric vertical motion, OLR and specific humidity over the eastern side of the low-pressure system, whereas the opposite lighter precipitation features are significant over the western side.

Another accompanying paper is under preparation for further description and dynamical understanding of statistically significant QBO modulations of global monsoon systems, such as the modulations of the Walker circulation along the equator over the western Pacific Ocean and the intensification (or weakening) of low-

pressure cyclonic circulations with a shift of precipitation patterns for a specific QBO-phase over the NH western Pacific Ocean during boreal summer and over the NH eastern Pacific and Atlantic Oceans during winter.

Acknowledgments

The authors are grateful for very useful discussion with and comments from Yukari Takayabu. The following funding sources are acknowledged: JSPS KAKENHI JP17H01159 and JSPS DG-RSTHE (Indonesia) Joint Research Program (SY), NSF grant AGS-1555851 (MHH).

Disclaimer : The contents and views expressed in this study are the views of the authors and do not necessarily reflect the views of the organizations they belong to.

References

Chang, C. P., Ding, Y., Lau, N. C., Johnson, R. H., Wang, B. and Yasunari, T. (Eds.), 2011, "The Global Monsoon System: Research and Forecast (2nd Edition)", *World Scientific Series on Asia-Pacific Weather and Climate*, **5**, p594.

Chang, C. P., Ha, K. J., Johnson, R. H., Kim, D., Lau, G. N. C. and Wang, B. (Eds.), 2020, "The Multiscale Global Monsoon System", *World Scientific Series on Asia-Pacific Weather and Climate*, **11**, p406.

Chang, C. P., Kuo, H. C., Lau, N. C., Johnson, R. H., Wang, B. and Wheeler, M. C. (Eds.), 2016, "The Global Monsoon System: Research and Forecast (3rd Edition)", *World Scientific Series on Asia-Pacific Weather and Climate*, **9**, p385.

Chang, C. P., Wang, B. and Lau, N. C. G. (Eds.), 2005, "The Global Monsoon System: Research and Forecast", WMO/TD, No.1266, p542. https://core.ac.uk/download/pdf/36730348.pdf.

Collimore, C. C., Hitchman, M. H. and Martin, D. W., 1998, "Is there a quasi-biennial oscillation in tropical deep convection?", *Geophys. Res. Lett.*, **25**, 333-336. https://doi.org/ 10.1029/97GL03722.

Collimore, C. C., Martin, D. W., Hitchman, M. H., Huesmann, A. and Waliser, D. E., 2003, "On the relationship between the QBO and tropical deep convection", *J. Climate*, **16**, 2552–2568. https://doi.org/10.1175/1520-0442(2003)016<2552:OTRBTQ> 2.0.CO;2.

Fan, F., Dong, X., Fang, X., Xue, F., Zheng, F. and Zhu, J., 2017, "Revisiting the relationship between the south Asian summer monsoon drought and El Niño warming pattern", *Atmos. Sci. Lett.*, **18**, 175-182. doi.org/10.1002/asl.740.

Geen, R., Bordoni, S., Battisti, D. S. and Hui, K., 2020, "Monsoons, ITCZs and the concept of the global monsoon", *Rev. Geophys.*, **58**, e2020RG000700. https://doi.org/10.1029/2020RG000700.

Haynes, P., Hitchcock, P., Hitchman, M., Yoden, S., Hendon, H., Kiladis, G., Kodera, K. and Simpson, I., 2021, "The influence of the stratosphere on the tropical troposphere", *J. Meteor. Soc. Japan*, **99**, 803-845. doi:10.2151/jmsj.2021-040.

He, C. and Li, T., 2019, "Does global warming amplify interannual climate variability?", *Climate Dynamics*, **52**, 2667-2684. doi:10.1007/s00382-018-4286-0.

He, C., Li., T., Zhou., W., 2020, "Drier north American monsoon in contrast to Asian-African monsoon under global warming", *J.Climate*, **33**, 9801-9816. doi:10.1175/jcli-d-20-0189.1.

Hitchcock, P., Haynes, P.H., Hitchman, M.H., Koh, T.Y., Sakazaki, T. and Yoden, S., 2019, "Report on the SATIO-TCS side meeting and related discussions atthe 6thSPARC General Assembly 2018", *SPARC newsletter*, **52**, 24-26.

Hitchman, M.H., Yoden, S., Haynes, P.H., Kumar, V. andTegtmeier, S., 2021,"An observational history of thedirect influence of the stratospheric quasi-biennialoscillation on the tropical and subtropical upper troposphereand lower stratosphere", *J. Meteor. Soc. Japan*,**99**, 239-267.doi:10.2151/jmsj.2021-012.

Huang, P. and Xie, S.P., 2015, "Mechanisms of change in ENSO-induced tropical Pacific rainfall variability in a warming climate", *Nature Geoscience,* **8**, 922-926.doi:10.1038/ngeo2571.

Krishnamurthy,V. and Goswami, B.N., 2000, "Indian monsoon-ENSO relationship on interdecadal timescale", *J.Climate*, **13**, 579-595.

Krishnamurti, T.N., Stefanova, L. and Misra, V., 2013, Chapter 5 Monsoons, in "Tropical Meteorology", Springer Atmospheric Sciences.Springer, 75-119.https://doi.org/10.1007/978-1-4614-7409-8_5.

Kumar, V., Yoden, S. and Hitchman, M.H., 2022, "QBO and ENSO effects on the mean meridional circulation, polar vortex, subtropical westerly jets and wave patterns during boreal winter", *J. Geophys. Res. Atmos.*, **127**,e2022JD036691. doi.org/10.1029/2022JD036691.

Lee H. T. and NOAA CDR Program, 2018, "NOAA Climate Data Record (CDR) of Monthly Outgoing Longwave Radiation (OLR), Version 2.7". NOAA National Centers for Environmental Information. https://doi.org/10.7289/V5W37TKD [access date, 2022/12/02].

Lee, J.H., Kang, M.J. and Chun, H.Y., 2019, "Differences in the tropical convective activities at the opposite phasesof the quasi-biennial oscillation",*Asia-Pacific J. Atmos. Sci.*,**55**, 317-336-https://doi.org/10.1007/s13143-018-0096-x-

Liess, S. and Geller, M.A., 2012,"On the relationshipbetween QBO and distribution of tropical deep convection", *J. Geophys. Res.*, **117**, D03108.doi:10.1029/2011JD016317.

Martin, Z., Son, S. W., Butler, A., Hendon, H., Kim, H.,Sobel, A., Yoden, S. andZhang, C., 2021, "The influence of the quasi-biennialoscillation on the Madden-Julianoscillation", *Nature Reviews Earth & Environment*, **2**, 477-489.https://www.nature.com/articles/s43017-021-00173-9.

NCAR (National Center for Atmospheric Research) Staff (Eds.), 2020, "The Climate Data Guide: GPCC: Global Precipitation Climatology Centre", Retrieved from https://climatedataguide.ucar.edu/climate-data/gpcc-global-precipitation-climatology-centre (last modified 27 Feb 2020).

Wallace, J.M., Panetta, R.L. and Estberg, J., 1993, "Representation of the equatorial stratospheric Quasi-Biennial Oscillation in EOF phase space", *J. Atmos. Sci.*, **50**, 1751-1762.https://doi.org/10.1175/1520-0469(1993)050<1751:ROTESQ>2.0.CO;2

Wang, B. and Ding, Q., 2008, "Global monsoon: Dominant mode of annual variation in the tropics", *Dyn. of Atmos. and Oceans*, **44**, 165-183.https://doi.org/10.1016/j.dynatmoce.2007.05.002.

Wang, B., Biasutti, M., Byrne, M.P., Castro, C., Chang, C.P., Cook, K., Fu, R., Grimm, A.M., Ha, K.J., Hendon, H., Kitoh, A., Krishnan, R., Lee, J. Y., Li J., Liu, J., Moise, A., Pascale, S., Roxy, M.K., Seth, A., Sui, C.H., Turner, A., Yang, S., Yun K.S., Zhang, L. and Zhou, T., 2021,"Monsoons climate change assessment",*B. Am. Meteorol. Soc.*,**102**, E1-E19, doi:10.1175/bams-d-19-0335.1.

Wang, P.X., Wang, B., Cheng, H., Fasullo, J., Guo, Z.T., Kiefer, T. and Liu, Z.Y., 2017, "The global monsoon across time scales: Mechanisms and outstanding issues", *Earth-Sci. Rev.*, **174**,84-121.https://doi.org/10.1016/j.earscirev.2017.07.006.

Wheeler, M.C. and Hendon, H.H., 2004, "An all-season real-time multivariate MJO index: Development of an index for monitoring and prediction", *Mon. Wea. Rev.*, **132**, 1917-1932. https://doi.org/10.1175/1520-0493(2004)132<1917:AARMMI>2.0.CO;2.

Yoden, S., Haynes, P.H., Hitchcock, P., Hitchman, M.H., Koh, T.Y., Sakazaki, T., Bal, S. and Rais A. F., 2020, "WCRP/SPARC SATIO-TCS joint workshop on stratosphere-troposphere dynamical coupling in the tropics", *SPARC newsletter*, **55**, 12-16.

Yoo, C. and Son, S. W., 2016, "Modulation of the boreal winter time Madden-Julian oscillation by the stratospheric quasi-biennial oscillation", *Geophys. Res. Lett.*, **43**, 1392-1398. https://doi.org/10.1002/2016GL067762.

Yu, S. Y., Fan, L., Zhang, Y., Zheng, X. T. and Li, Z., 2021, "Re-examining the Indian summer monsoon rainfall–ENSO relationship from its recovery in the 21st century: Role of the Indian Ocean SST anomaly associated with types of ENSO evolution", *Geo. Res. Lett.*, **48**, e2021GL092873, doi.org/10.1029/2021GL092873.

Yun, K. S. and Timmermann, A., 2018, "Decadal monsoon-ENSO relationships re-examined", *Geo. Res. Lett.*, **45**, 2014-2021. doi.org/10.1002/2017GL07691.